Ullah, S.; Ullah, H.; Bouhjar, F.; Mollar García, MA.; Marí, B. (2018). Synthesis of in-gap band CuGaS2:Cr absorbers and numerical assessment of their performance in solar cells. Solar Energy Materials and Solar Cells. 180:322-327. https://doi.org/10.1016/j.solmat.2017.06.062

S. Ullah, H. Ullah, F. Boujhar, M. Mollar, B. Marí; Solar Energy Materials and Solar Cells, **180**(2018)322
https://doi.org/10.1016/j.solmat.2017.06.062

Synthesis of in-gap band $CuGaS_2$:Cr absorbers and numerical assessment of their performance in solar cells

Shafi Ullah, Hanif Ullah, Feriel Bouhjar, Miguel Mollar, Bernabé Marí*

Departament de Física Aplicada-IDF, Universitat Politècnica de València, Camí de Vera s/n, 46022-València, Spain

*Corresponding author: bmari@fis.upv.es (B. Marí)

Abstract

$CuGaS_2$ thin films were obtained by sulfurization of $CuGaSe_2$. $CuGaSe_2$ thin films were first electrodeposited from aqueous solutions containing $CuCl_2$, $GaCl_3$, and H_2SeO_3 and subsequently annealed at 400 °C for 10 min in forming gas atmosphere and in the presence of molecular sulfur. This sulfurization process resulted in the complete conversion of $CuGaSe_2$ into $CuGaS_2$. The formation of $CuGaS_2$ was proven by X-Ray diffraction and optical spectroscopy. Diffraction peaks of $CuGaS_2$ shifted to higher angles than those observed for $CuGaSe_2$ films, and the optical band gap shifted to blue rising from 1.66 eV for $CuGaSe_2$ to 2.2 eV for $CuGaS_2$. When Cr ions were added to the initial electrolyte, the final $CuGaS_2$ films exhibited a broad in-gap absorption band centred at 1.63 eV that can be ascribed to Cr atoms in Ga sites. The performance of solar cells based on $CuGaS_2$:Cr absorbers containing an in-gap absorption band was then estimated by numerical simulation using Solar Cell Capacitance Simulator Software. Both quantum efficiency and short circuit current of simulated Mo/$CuGaS_2$:Cr/CdS/ZnO solar cells rose up proportionally to the amount of Cr present in $CuGaS_2$:Cr absorbers. As a result, the photo conversion efficiency of the simulated devices changed from 14.7% for $CuGaS_2$ to 34% for $CuGaS_2$:Cr absorbers. Nevertheless, when neutral defects related to Cr-doping were introduced in the absorber layer, the positive effect of the enhancement of photon harvesting due to IGB was compensated by a decline in the carrier collection and the overall efficiency of the device fell considerably.

Keywords: $CuGaS_2$**;** thin film solar cells; intermediate band solar cell; numerical simulation; photoconversion efficiency; SCAPS.

1. Introduction

CIGS Chalcopyrite semiconductors are one of the promising materials to be used in high-performance photovoltaic devices due to their direct bandgap, which can be tuned between 1.1 for $CuInSe_2$ and 2.2 eV for $CuGaS_2$. Also, their cost-effectiveness and easy processing are well known. Recently, CIGS thin-film photovoltaic devices reached a record solar efficiency of 22.3% [1]. Among thin film technologies, CIGS solar cells have achieved highest conversion efficiencies at laboratory scale [2, 3]. Efforts to seek an economical and scalable method for the production of stoichiometric CIGS thin-films have been going on to allow the commercialization of these devices. Among several techniques, electrodeposition has demonstrated to produce CIGS devices with high efficiency [4]. Currently efforts are being made to increase the thin film efficiency to the theoretical determination as well as to improve inexpensive deposition strategies for the chalcopyrite absorber layer [5].

The band gap energy of semiconductor materials plays a key role in performance of photovoltaic devices [6]. According to the Shockley–Queisser limit the optimal band gap energy of single band gap PV device was calculated to be about 1.4 eV [7]. Therefore, it would be unreasonable to use $CuGaS_2$ thin film as absorber in photovoltaic devices based on one junction due to their high band gap which is about 2.2 eV. However, this energy matches the optimal bandgap well to host an in-gap band (IGB) (also known as intermediate band) intended to absorb photons with energies lower than the gap. In the proposed IGB material electrons can follow two ways to be promoted from the valence band to the conduction band: a) absorbing a photon with energy higher than the bandgap, and b) through the absorption of two photons with energy below the bandgap. The absorption of one photon promotes one electron from the valence band to the partially filled IGB and then the electron is transferred from this IGB to the conduction band after the absorption of a second photon. This may allow a more efficient use of the solar spectrum in photovoltaic devices. This type of solar cells would be able to utilize the solar spectrum more efficiently, resulting in a theoretical efficiency limit of 63.2% [8], which is significantly higher than the 40.7% limit of conventional single band-gap photovoltaic cells [7]. Such devices would possess higher open circuit voltages and increased short circuit currents due to the higher band gap energy of the absorbing material and the greater absorption coming from sub-band gap photons, resulting in an increase of the overall efficiency [9].

According to the literature [10], chrome substituting Ga in $CuGaS_2$ chalcopyrite lattices would generate an IGB separated from both valence and conduction bands. When the transition metal (Cr) IGB is introduced into the $CuGaS_2$ lattice it produces a partially filled band separated from both conduction and valence bands that allows promoting electron-hole pairs through a two photons absorption process with sub bandgap energies. Therefore, the use of an IGB absorber would allow harvesting higher amounts of solar photons.

The main determination of the present work is to dope $CuGaS_2$ thin films with the transition-metal Cr to create a suitable IGB absorber [11]. Herein, we report the synthesis and optical characterization of $CuGaS_2$ and $CuGaS_2$:Cr thin films containing an IGB associated to Cr. $CuGaS_2$ thin films were produced by sulfurization of previously electrodeposited $CuGaSe_2$ films. The replacement of Se by S was completely substituted after sulfurization. Optical analysis showed that the band gap shifted from 1.66 for $CuGaSe_2$ to 2.20 eV for $CuGaS_2$.with the sulfurization, the position of X-Ray diffractograms peaks also shifted from 27 to 29 degrees. The effectiveness of Cr-doping was inferred from the presence of Cr in $CuGaS_2$ layers detected by microanalysis and the optical detection of an in-gap absorption band. Furthermore, the behaviour of photovoltaic devices, based on $CuGaS_2$ absorbers with and without an IGB, was calculated specific Solar Cell Capacitance Simulation (SCAPS) software [12].

2. Experimental

$CuGaSe_2$ layers were electrodeposited from an electrolyte solution containing 2 mMol L^{-1} $CuCl_2$, 4 mmol L^{-1} H_2SeO_3, 10mmol L^{-1} $GaCl_3$, 50mmol L^{-1} KSCN, 100 mmol L^{-1} NH_4Cl and 300 mmol L^{-1} LiCl. The precursor solution pH was adjusted between 2.3 and 2.4 by adding hydrochloric acid (HCl) and potassium hydroxide (KOH). For better stability of the deposition bath solution LiCl was used as a supporting electrolyte, also improving the quality of the deposited layers.

Electrodeposition was performed on a standard 3-electrode electrochemical cell. The $CuGaSe_2$ thin films were deposited onto a 1μm thick Mo-coated soda lime glass substrate acting as a working electrode, a platinum wire was used as counter electrode and Ag/AgCl as reference electrode.

For doping purposes, Cr^{3+} ions were added to the electrolyte described above. 150 mMol L^{-1} of $Cr(ClO_4)_3$ was dissolved in 40 mL of the electrolyte aqueous solution. The pH of the final solution was adjusted between 2.3 and 2.4 using concentrated HCl. Electrodeposition produced

Cr-doped $CuGaSe_2$ films and these films, which were subsequently sulfurized following the sulfurization procedure described below.

$CuGaS_2$ layers were obtained after subsequent sulfurization of previously electrodeposited $CuGaSe_2$ layers. A complete replacement of the selenium by sulfur, transforming the precursor $CuGaSe_2$ wurtzite film into a $CuGaS_2$ chalcopyrite film took place in a quartz tube kept inside a cylindrical oven at a temperature of 400 ºC for 10 minutes in forming gas atmosphere.

The crystal structure of $CuGaSe_2$ and $CuGaS_2$ thin films were investigated by X-Ray Diffraction (XRD) with a Rigaku Ultima IV diffractometer in the Bragg-Brentano configuration using CuKα radiation (λ=1.54060 Å). The chemical composition was analysed by means of Energy Dispersive Spectroscopy (EDS) with a FESEM Zeiss model Ultra55.

Numerical simulations were performed using SCAPS, which is a one dimensional computer software to simulate electrical characteristics of thin film heterojunction solar cells. SCAPS was developed for CIGS and CdTe thin film solar cells but it has been applied to other thin film materials [13]. $CuGaS_2$:Cr absorber layers with different Cr contents were used in the simulation. Besides, the effect of neutral defects related to Cr-doping on the performance of solar cells was also studied and discussed.

3. Results and discussion

Figure 1 shows the XRD patterns of $CuGaSe_2$ and $CuGaS_2$ thin films at their different preparation stages: (a) electrodeposited $CuGaSe_2$ thin films and (b) sulfurized $CuGaSe_2$ thin films annealed for 10 minutes at 450 ºC. The diffractogram obtained for $CuGaSe_2$ thin films matches the tetragonal crystal system JCPDS No. 075-0104 pattern well. The major peaks were located at 27.9°, 45.7°/46.2° and 54.3°/55.2° corresponding to (1 1 2), (2 2 0)/(2 0 4) and (3 1 2)/(1 1 2) diffraction planes, respectively.

The sulfurization process of the electrodeposited $CuGaSe_2$ films took place after a short annealing time in presence of molecular sulfur, resulting in the formation of the $CuGaS_2$ chalcopyrite phase as revealed by the XRD pattern of sulfurized films, [Figure 1 (b)]. The XRD peaks shifted to higher angles with the sulfurization process. The main XRD peak corresponding to (1 1 2) diffraction peaks shifted from 27.9 to 29.0 degrees. Furthermore, the peaks corresponding to (2 2 0) and (2 0 4) and (3 1 2) and (1 1 6) diffraction planes observed for annealed $CuGaSe_2$ films also shifted to higher angles for sulfurized films. These XRD peaks match the JCPDS No. 75-0103 pattern corresponding to $CuGaS_2$ films. This diffraction pattern

confirms the replacement of Se atoms by S atoms after sulfurization, and consequently, $CuGaSe_2$ thin films were transformed into $CuGaS_2$ [14,15,16].

Both $CuGaSe_2$ and $CuGaS_2$ films exhibited a tetragonal crystalline structure. The XRD patterns of $CuGaSe_2$ and $CuGaS_2$ thin films display a highly crystalline structure, offering the possibility of being used for photovoltaic devices with high conversion efficiency [17].

EDS was used to estimate the composition of deposited $CuGaSe_2$ and $CuGaS_2$ films. Figure 2 (a, b) shows the EDS spectra of annealed $CuGaSe_2$ and $CuGaSe_2$ films doped with chrome. Main X-ray peaks belong to Cu, Ga, Se and Mo, produced by the substrate. In Cr-doped $CuGaSe_2$ films, three lines located at 0.5, 5.5 and 6.0 keV, respectively, support the presence of chrome in these samples. After sulfurization the lines related to Se practically disappear, which means that the substitution of selenium by sulfur took place [18]. Only a residual part of selenium (below 1%) remains after 10-minute sulfurization. The content of chrome in doped films always remains between 1 and 2%, irrespective of the amount of Cr^{3+} added to the starting electrolyte, which means that the Cr:Ga ratio ranges from 4 to 8%.

Figure 3 shows the normalized absorbance for $CuGaSe_2$, $CuGaS_2$ and $CuGaS_2$:Cr thin films, respectively. According to Figure 3 (a), the cut-off wavelength for $CuGaSe_2$ is about 746 nm, which corresponds to a bandgap of 1.6 eV. Figure 3 (b) displays the normalized absorbance for $CuGaS_2$ films after sulfurization treatment. The cut-off wavelength for $CuGaS_2$ films shifts to a lower wavelength (563 nm), which means a higher energy bandgap (2.2 eV). Figure 3 (c) shows the normalized absorbance for $CuGaS_2$:Cr thin films. An additional characteristic with respect to undoped $CuGaS_2$ films is evidenced: in $CuGaS_2$:Cr films, a wide absorption band centered at 760 nm (1.63 eV) appears. This absorption band can be assigned to a sub-band related to Cr-doping. According to theoretical studies, the substitution Ga^{3+} by some transition metals like Cr would give rise to a partially filled absorption band into $CuGaS_2$ chalcopyrite structures, which would then support the promotion of electrons from the valence band to the conduction band through a two-photon absorption procedure [19].

The proposed in-gap band concept has gained a great deal of attention in the field of third generation solar cell research. The IGB position should neither overlap with the valence band (VB) nor with the conduction band (CB). Such an in-gap band does not only absorb photons having an energy higher than that of the band gap (Eg) but also permits the absorption of photons corresponding to the sub-band gap, which are capable to promote electrons from the VB to the IGB and then from the IGB to the CB [20]. The IGB associated to Cr-doped $CuGaS_2$

may allow a higher current to be obtained at the voltage corresponding to the energy gap value, which is described in detail in the simulation part.

4. Numerical simulation of solar cells based on $CuGaS_2$:Cr absorbers.

The performance of photovoltaic devices based on IGB-absorbers has been numerically simulated using SCAPS. The simulated photovoltaic device consists of the following sequence of layers: Mo/$CuGaS_2$:Cr/CdS/ZnO corresponding to back contact, absorber, buffer and window layers, respectively.

In the simulation we used the experimental absorption coefficient measured for $CuGaS_2$:Cr considering that 5% of Ga was substituted by Cr. To further estimate the effectiveness of the Cr-related IGB, we proportionally increased the Cr content to 10% and 20% and then studied its effect on the performance of the solar cell.

Figure 4 shows the energy band diagram for Mo/$CuGaS_2$:Cr/CdS/ZnO thin film solar cells. The diagram plots various key electron energy levels as the Fermi level and the energy band edges. The band gap of pure $CuGaS_2$ is 2.2 eV, which is appropriate for hosting an IGB separated from both conduction and valence bands. Cr doping originates an IGB centered at 1.63 eV, which enhances the absorption and allows boosting the efficiency of the device.

Figure 5 shows the External Quantum Efficiency (EQE) under AM1.5 illumination for $CuGaS_2$:Cr solar cells with a different Cr content ranging from 0 to 20%. The EQE is the ratio of the amount of charge carriers collected by the solar cell with respect to the amount of incident photon energy on the solar cell. The EQE for pure $CuGaS_2$ falls to zero for wavelengths longer than 620 nm, which corresponds to the band gap of the absorber (2.2 eV). However, due to the absorption of the IGB, a rise in EQE is observed within the 620-1000 nm range. This increase in EQE is related to the absorption of sub-band gap photons associated to the IGB and the general rule is: the higher the Cr content, the higher the EQE in the region below the band gap. The key goal of this research was to improve the performance of solar cells by inserting an IGB to cover a wider wavelength range.

Figure 6 shows the J-V characteristic of solar cells for $CuGaS_2$ absorbers with various Cr contents. Under AM1.5 illumination, the short circuit current (J_{sc}) depends on the Cr content in the $CuGaS_2$ absorber layer. The short circuit current increases with regard to the Cr percentage. For Cr 0%, the $CuGaS_2$ absorber gives J_{sc}=12.6 mA/cm^2, and J_{sc} increases proportionally to the Cr content of up to 29.41 mA/cm^2 for Cr 20%. Cr 5%, 10%, and 20% means that the remaining Ga atoms are 95, 90 and 80% with respect to Ga atoms in pure $CuGaS_2$ absorbers assuming that

all Cr atoms are substituting Ga atoms. Unfortunately, this cannot be inferred from EDS analysis.

Table 1 displays the main photovoltaic parameters for the studied devices in relation to the Cr content. Both, the open circuit voltage (Voc=1.34 V) and the fill factor (FF=89.5) remain constant with the amount of Cr. However, the short circuit current (Jsc) dramatically increases with the Cr content, and as a result the photo conversion efficiency (PCE) increases from 14.73% for the $CuGaS_2$ absorber layer without Cr to 34.00% for $CuGaS_2$:Cr (20%) absorbers. This increase in the PCE is directly related to the effectiveness of the intermediate band for absorbing photons with energies below the band gap.

In the $CuGaS_2$ lattice, Cr atoms should act as a neutral defect and would then hinder the movement of the carriers. Therefore, Cr doping add two effects; a) increasing the photon harvesting through the related IGB, and b) hindering the carriers drift as the doping modifies the crystal lattice. In order to take into account both effects, we calculated the photovoltaic parameters for $CuGaSe_2$:Cr devices for an increasing concentration of neutral defects.

Figure 7 shows the J-V curves for PV devices based on $CuGaSe_2$:Cr absorbers with an increasing concentration of Cr-related neutral defects. Several features can be seen in these J-V curves: a) increasing neutral defects results in a drop of Voc, b) Jsc is also decreased as the number of neutral defects increases. As a result, PCE drops drastically with the amount of neutral defects. The photovoltaic parameters of such devices in relation to the neutral defects concentration are summarized in Table 2.

By introducing neutral defects, the relationship between the PCE and defects is inverse. When the neutral defect concentration increases from 10^{16} to 10^{20} cm^{-3}, the PCE decreases from 34 to 2.3%, which means that the performance of the photovoltaic device is very sensitive to neutral defects. Cr-doping improves photon harvesting and, consequently, the short circuit current but, simultaneously, spreads the concentration of neutral defects that obstruct the extraction of carriers to the external load.

5. Conclusions

$CuGaS_2$ thin films were obtained by sulfurization at 400 ºC for 10 min of previously electro-deposited $CuGaSe_2$ precursor films. The shift observed in X-ray diffraction peaks and the widening of the optical bandgap from 1.66 to 2.20 eV confirm the conversion of $CuGaSe_2$ into $CuGaS_2$.

After partial substitution of Ga by Cr atoms an absorption band below the gap is observed. This in-gap band is centered at about 1.63 eV above the valence band. Apart from transitions from the VB to the CB, the IGB band in $CuGaS_2$:Cr films allows the absorption of two sub-band gap photons and promotes electrons from the VB to the CB via the intermediate IGB. As a result, the absorption coefficient of the IGB absorber extends to longer wavelength region.

Using the experimental absorption coefficient obtained for $CuGaS_2$:Cr films with 5% of Ga atoms being substituted by Cr, we performed numerical simulations to assess the behavior of a solar cell based on $CuGaS_2$:Cr absorbers for various amounts of Cr. The absorption due to the IGB dramatically increases the short circuit current of the solar cell, and the photo conversion efficiency also grows from 14.7% for the $CuGaS_2$ absorber layer without Cr to 34% for the $CuGaS_2$:Cr absorber layer with 20% Cr content. However, as the amount of neutral defects related to Cr increases, the efficiency of devices diminishes, showing that the PCE for IGB-absorbers is very sensitive to the presence of neutral defects.

Acknowledgments

This work was supported by Ministerio de Economía y Competitividad (ENE2016-77798-C4-2-R) and Generalitat Valenciana (Prometeus 2014/044).

TABLES

Table 1: Output parameters of the modeled Mo/$CuGaS_2$:Cr/CdS/ZnO thin film solar cell with various Cr content.

Cr (%)	Voc (Volt)	Jsc (mA/cm^2)	FF (%)	PCE (%)
0	1.344	12.22	89.7	14.73
5	1.339	20.31	89.5	24.35
10	1.341	23.38	89.5	28.07
20	1.343	29.41	89.5	34.00

Table 2: Output parameters of the modeled Mo/$CuGaS_2$Cr/CdS/ZnO thin film solar cell with neutral defects.

Neutral Defects (cm^{-3})	Voc (Volt)	Jsc (mA/cm^2)	FF (%)	PEC (%)
0	1.34	29.41	89.70	34.00
10^{16}	1.34	29.32	70.90	30.29
10^{17}	1.30	26.48	51.71	17.80
10^{18}	1.27	23.92	42.70	12.97
10^{19}	1.21	21.74	38.82	10.21
10^{20}	1.10	7.80	26.34	2.26

FIGURE CAPTIONS

Figure 1. XRD patterns of $CuGaSe_2$ and $CuGaS_2$ films: (a) $CuGaSe_2$ after annealing at 400 ºC in forming gas atmosphere, and (b) after sulfurization in molecular sulfur for 10 minutes at 400 ºC.

Figure 2. EDS spectrum for: a) annealed $CuGaSe_2$ b) $CuGaSe_2$ doped with Cr.

Figure 3. Comparison of the absorbance of $CuGaSe_2$, $CuGaS_2$ and $CuGaS_2$:Cr thin films. The broad absorption band observed for $CuGaS_2$:Cr, centred at 760 nm, is attributed to the Cr-related in-gap band.

Figure 4. Band diagram of the Mo/$CuGaS_2$/CdS/ZnO thin film solar cell.

Figure 5. EQE for Mo/$CuGaS_2$:Cr/CdS/ZnO solar cells with different Cr contents under standard AM1.5 illumination.

Figure 6. J-V characteristics of $CuGaS_2$:Cr thin film solar cells with various Cr contents.

Figure 7. J-V characteristics of solar cells based on $CuGaS_2$:Cr 20% absorbers with different amounts of neutral defects.

FIGURES

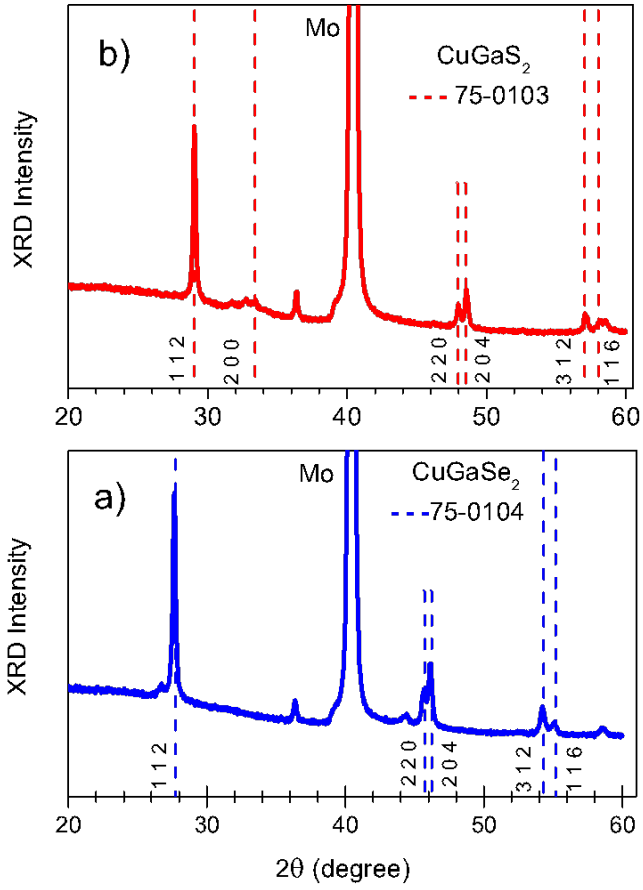

FIGURE 1. XRD patterns of $CuGaSe_2$ and $CuGaS_2$ films: (a) $CuGaSe_2$ after annealing at 400 ºC in forming gas atmosphere, and (b) after sulfurization in molecular sulfur for 10 minutes at 400 ºC.

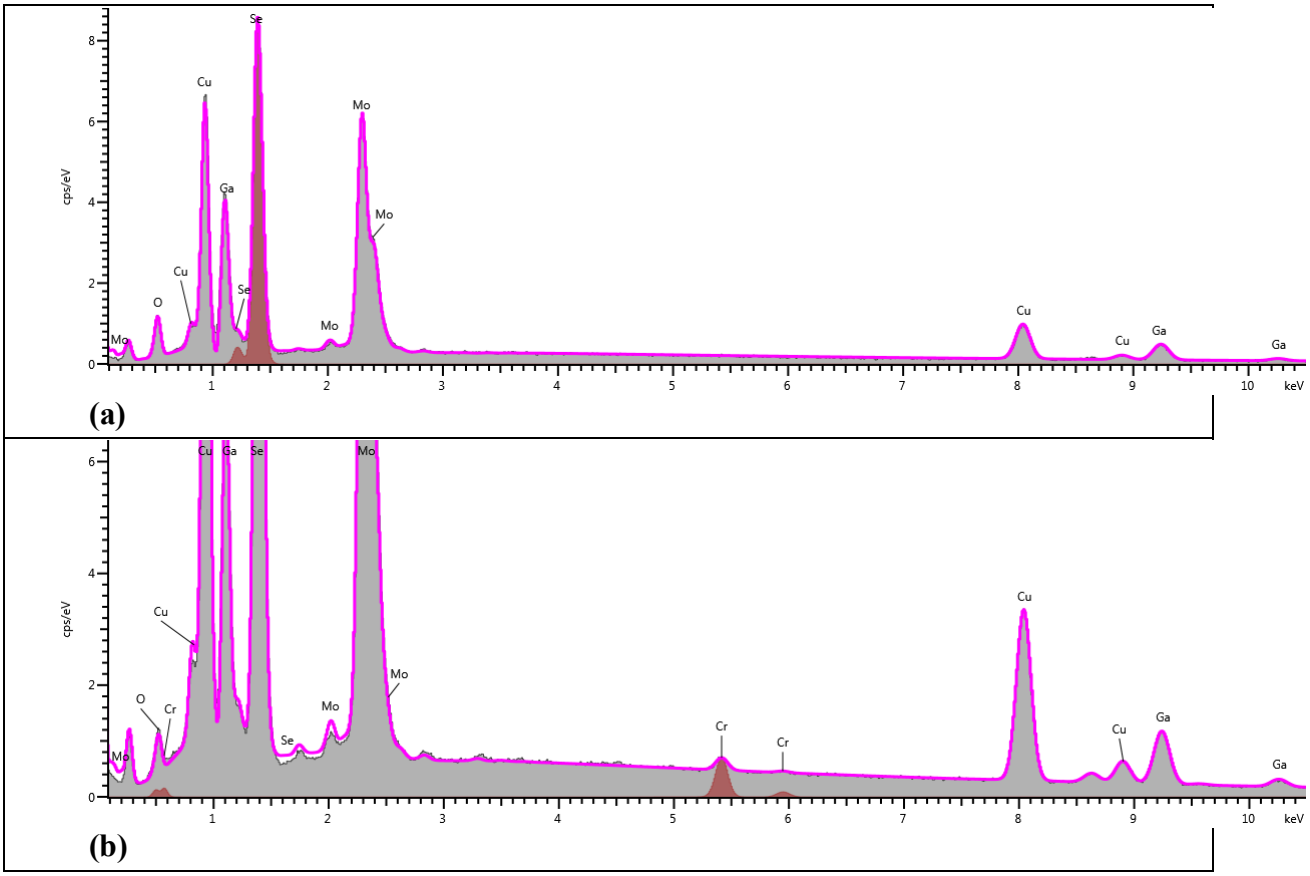

Figure 2. EDS spectrum for: a) annealed $CuGaSe_2$, b) $CuGaSe_2$ doped with Cr.

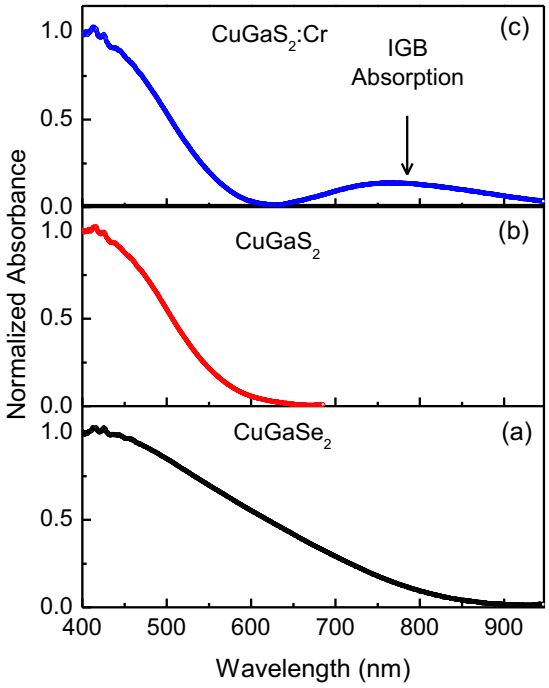

Figure 3. Comparison of the absorbance of $CuGaSe_2$, $CuGaS_2$ and $CuGaS_2$:Cr thin films. The broad absorption band observed for $CuGaS_2$:Cr, centred at 760 nm, is attributed to the Cr-related in-gap band.

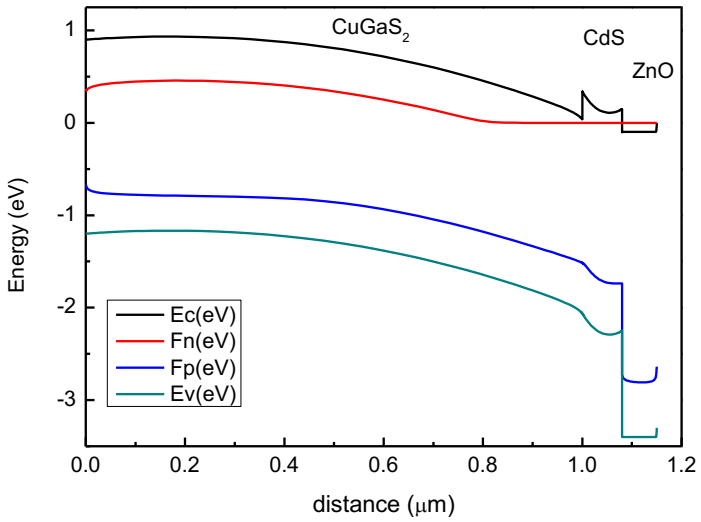

Figure 4. Band diagram of the Mo/$CuGaS_2$/CdS/ZnO thin film solar cell.

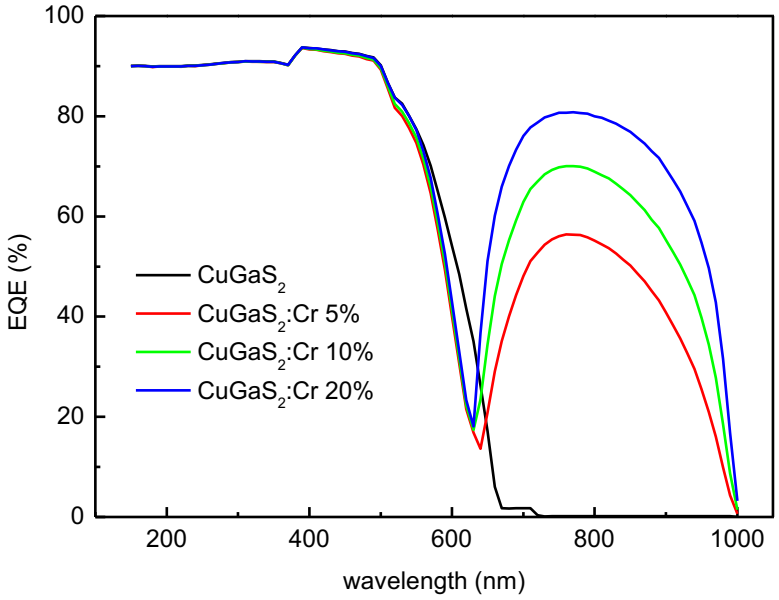

Figure 5. EQE for Mo/$CuGaS_2$:Cr/CdS/ZnO solar cells with different Cr contents under standard AM1.5 illumination.

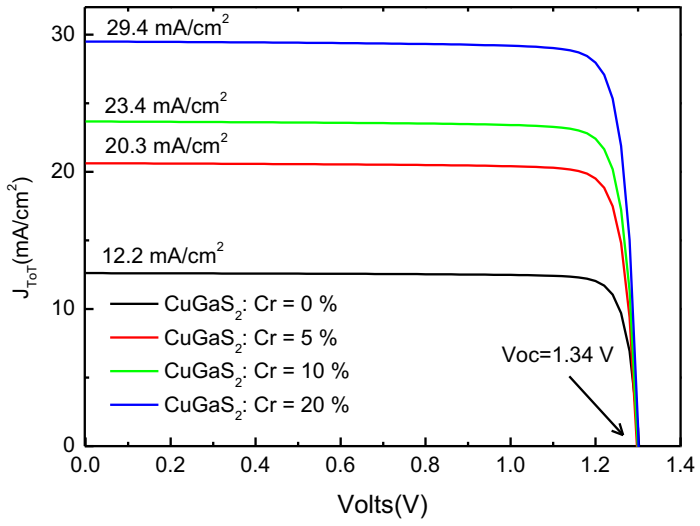

Figure 6. J-V characteristics of $CuGaS_2$:Cr thin film solar cells with various Cr contents.

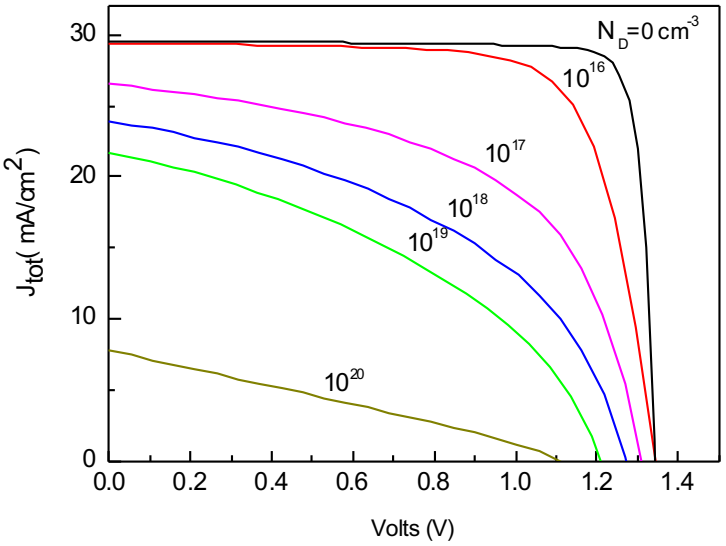

Figure 7. J-V characteristics of solar cells based on $CuGaS_2$:Cr 20% absorbers with different amounts of neutral defects.

REFERENCES

[1] Mezher, M., Garris, R., Mansfield, L. M., Horsley, K., Weinhardt, L., Duncan, D. A., ... & Heske, C. (2016). Electronic structure of the Zn (O, S)/Cu (In, Ga) Se2 thin-film solar cell interface. Progress in Photovoltaics: Research and Applications; 24, 1142-1148

[2] Carrete, A., Placidi, M., Shavel, A., Pérez-Rodríguez, A., & Cabot, A. (2015). Spray-deposited CuIn1− xGaxSe2 solar cell absorbers: Influence of spray deposition parameters and crystallization promoters. physica status solidi (a), 212(1), 67-71.

[3] Saji, V. S., Choi, I. H., & Lee, C. W. (2011). Progress in electrodeposited absorber layer for $CuIn_{(1-x)}Ga_xSe_2$ (CIGS) solar cells. Solar Energy, 85(11), 2666-2678.

[4] Aksu, S., Pethe, S., Kleiman-Shwarsctein, A., Kundu, S., Pinarbasi & M., in: 38th IEEE Photovotaics Specialists Conference, (2012) 3092-3097.

[5] Saji, V. S., Lee, S. M., & Lee, C. W. (2011). CIGS thin film solar cells by electrodeposition. Journal of the Korean Electrochemical Society, 14(2), 61-70.

[6] Wang, W., Yang, J., Zhu, X., & Phillips, J. (2011). Intermediate-band solar cells based on dilute alloys and quantum dots. Frontiers of Optoelectronics in China, 4(1), 2-11.

[7] Shockley, W., & Queisser, H. J. (1961). Detailed balance limit of efficiency of p-n junction solar cells. Journal of applied physics, 32(3), 510-519.

[8] Luque, A., & Martí, A. (1997). Increasing the efficiency of ideal solar cells by photon induced transitions at intermediate levels. Physical Review Letters, 78(26), 5014.

[9] Palacios, P., Sánchez, K., Conesa, J. C., & Wahnón, P. (2006). First principles calculation of isolated intermediate bands formation in a transition metal-doped chalcopyrite-type semiconductor. Physica Status Solidi (a), 203(6), 1395-1401.

[10] Palacios, P., Sánchez, K., Conesa, J. C., Fernández, J. J., & Wahnón, P. (2007). Theoretical modelling of intermediate band solar cell materials based on metal-doped chalcopyrite compounds. Thin Solid Films, 515(15), 6280-6284.

[11] Aguilera, I., Palacios, P., & Wahnón, P. (2010). Enhancement of optical absorption in Ga-chalcopyrite-based intermediate-band materials for high efficiency solar cells. Solar Energy Materials and Solar Cells, 94(11), 1903-1906.

[12] Burgelman, M., Verschraegen, J., Degrave, S., & Nollet, P. (2004). Modeling thin-film PV devices. Progress in Photovoltaics: Research and Applications, 12(2-3), 143-153.

[13] Ullah, H., & Marí, B. (2014). Numerical analysis of SnS based polycrystalline solar cells. Superlattices and Microstructures, 72, 148-155.

[14] Kim, D., Kwon, Y., Lee, D., Yoon, S., Lee, S., & Yoo, B. (2015). The Effect of Sulfurization Temperature on CuIn (Se, S) 2 Solar Cells Synthesized by Electrodeposition. Journal of the Electrochemical Society, 162(1), D36-D41.

[15] Hou, W. W., Bob, B., Li, S. H., & Yang, Y. (2009). Low-temperature processing of a solution-deposited CuInSSe thin-film solar cell. Thin Solid Films, 517(24), 6853-6856.

[16] Lee, J., Lee, W., Shrestha, N. K., Lee, D. Y., Lim, I., Kang, S. H., … & Han, S. H. (2014). Influence of encapsulated electron active molecules of single walled-carbon nanotubes on superstrate-type Cu (In, Ga) Se 2 solar cells. Materials Chemistry and Physics, 144(1), 49-54.

[17] Yang, J., Lee, D., Huh, K., Jung, S., Lee, J., Lee, H., … & Kim, G. (2015). Influence of surface properties on the performance of Cu(In, Ga)(Se, S)$_2$ thin-film solar cells using Kelvin probe force microscopy. RSC Advances, 5(51), 40719-40725.

[18] Ullah, S., Mollar, M., & Marí, B. (2016). Electrodeposition of $CuGaSe_2$. Journal of Solid State Electrochemistry, 20(8), 2251-2257.

[19] Palacios, P., Aguilera, I., Wahnón, P., & Conesa, J. C. (2008). Thermodynamics of the formation of Ti-and Cr-doped $CuGaS_2$ intermediate-band photovoltaic materials. The Journal of Physical Chemistry C, 112(25), 9525-9529.

[20] Ullah, H., Ullah, S., & Soucase, B. M. (2014, November). Baseline of numerical simulations for ZnTe based thin-film solar cells. In Energy Systems and Policies (ICESP), 2014 International Conference on (pp. 1-6). IEEE.